Solid Electrolyte Based Galvanic Cell for Measuring the Antimony Concentration in Molten Zinc

Jeffrey W. Fergus* **and Shiqiang Hui****

Materials Research and Education Center, Auburn University, Auburn, Alabama 36849, USA

ABSTRACT

A concept for a sensor to monitor the antimony concentration in molten zinc has been tested. The sensor consists of a stabilized zirconia solid electrolyte with a $ZrSb_2$ auxiliary electrode to provide the sensitivity to antimony. Electromotive force measurements of the antimony activity in molten zinc using this cell are in agreement with values calculated from measurements of the zinc activity in zinc-antimony alloys. However, the lifetime of the sensor is limited due to reaction of the $ZrSb_2$ auxiliary electrode with the molten zinc to form zirconium-zinc intermetallic compounds.

Introduction

Control of the zinc alloy composition during hot-dip galvanization is critical in controlling the crystallization and flow characteristics of the molten zinc and thus can be used to control the appearance and properties of the resulting galvanized coating.[1] Information on the zinc alloy composition during galvanization could be used to make on-line adjustments of the processing conditions and thus improve the quality of the galvanized product. Although either lead or antimony can be used to control the galvanization process, the use of antimony has become more prevalent due to concerns over the environmental effects of lead. Thus, a sensor which could measure the concentration of antimony in molten zinc would be useful in improving process control during the hot-dip galvanization of steel sheet.

A simple potentiometric antimony sensor would require an antimony-ion conducting solid electrolyte, which has not been reported. However, through the use of an auxiliary electrode, the activity an element other than that which is mobile in the electrolyte can be measured.[2] For example, the activity of nickel in copper has been measured using an oxide-ion conducting electrolyte (*i.e.*, stabilized zirconia) with the addition of nickel oxide as an auxiliary electrode.[3] An oxide-ion conducting electrolyte is used to measure the oxygen partial pressure established by the equilibrium between nickel (in copper) and nickel oxide, which depends on the activity of nickel in the copper alloy. Stabilized zirconia electrolytes have been used to measure the free-energy of formation of antimony oxide (Sb_2O_3) by measuring the oxygen partial pressure in equilibrium with pure antimony.[4,5] Equilibration of Sb_2O_3 with antimony at a reduced activity (*i.e.*, in an alloy) would establish an oxygen partial pressure which is higher than that established by the equilibration of Sb_2O_3 with pure antimony. The difference between these two oxygen partial pressures is determined by the difference between the two antimony activities, so the addition of Sb_2O_3 could be used as an auxiliary electrode for an antimony sensor.

One requirement for electromotive force (EMF) measurements is that the electrolyte and electrode materials are chemically stable in the operating environment. Thus, EMF measurements can easily be used to measure the more active element in an alloy. For example, molten chloride electrolytes have been used to measure the activities of tin,[6] gallium,[7] and aluminum[8,9] in zinc. However, Sb_2O_3 is less stable than zinc oxide (ZnO), [10] so the molten zinc would reduce the Sb_2O_3 by forming ZnO, and the electrode would become insensitive to the antimony activity. Alternatively, a mixed oxide, such as $Zn_7Sb_2O_{12}$ or $ZnSb_2O_6$, [11-13] could be used as the auxiliary electrode, but because of the near unit activity of zinc in a hot-dip galvanization bath, the sensor output would respond to zinc activity rather than antimony activity. Molten chloride electrolytes have been used to measure the activity of zinc in Zn-Sb [14] and Zn-Sb-Ag [15] alloys. However, the zinc activity does not change significantly in zinc alloys containing small antimony concentrations, so a sensor for the *in situ* measurement of the antimony composition is needed. Galvanic cells with solid halide electrolytes and antimony halide auxiliary electrodes would be sensitive to antimony, but would likely be reduced by molten zinc. In addition, the antimony halides melt below room temperature[16] and would thus likely have significant vapor pressures at the elevated temperatures in molten zinc.

An alternative approach to developing an antimony sensor is to use an antimony-containing intermetallic as the auxiliary electrode. Fortunately, antimony forms intermetallic compounds with elements such as zirconium,[17-20] lanthanum,[21] magnesium,[21] calcium,[22,23] and barium,[24,25] all of which also form compounds which are solid electrolytes (*i.e.*, ZrO_2, LaF_3, MgF_2, CaF_2, BaF_2). A Zr-Sb intermetallic is the most promising auxiliary electrode material, since stabilized zirconia is the most common solid electrolyte. The addition of the most antimony-rich intermetallic, $ZrSb_2$, to the sensing electrode would result in reaction 1

$$ZrO_2 + 2Sb = ZrSb_2 + O_2 \quad [1]$$

If the activities of ZrO_2 and $ZrSb_2$ are unity or constant (*i.e.*, the activity of ZrO_2 in stabilized zirconia is slightly less than unity) the oxygen partial pressure (p_{O_2}) is related to the antimony activity (a_{Sb}) by a constant (K)

$$p_{O_2} = K a_{Sb}^2 \quad [2]$$

so the cell voltage according to the Nernst equation becomes

$$E = \frac{RT}{4F} \ln \left(\frac{p_{O_2}^R}{K a_{Sb}^2} \right) \quad [3]$$

where R is the gas constant, F is Faraday's constant, T is the temperature, and $p_{O_2}^R$ is the reference oxygen partial. The reference oxygen potential can be established using a gas (*e.g.*, air), condensed phase (*e.g.*, metal + metal oxide), or, with the addition of $ZrSb_2$, a fixed antimony activity. In the latter case, the reference potential is established by reaction 1, so the EMF for cell I (Eq. 3) simplifies to

$$E = \frac{RT}{2F} \ln \left(\frac{a_{Sb}^{\text{reference}}}{a_{Sb}^{\text{alloy}}} \right) \quad [4]$$

where $a_{Sb}^{\text{reference}}$ and a_{Sb}^{alloy} are the antimony activities at the reference and working electrodes, respectively.

Analogous reactions can be established for the other intermetallic compounds mentioned above with the corresponding solid electrolytes. In the work described here, a zirconia electrolyte has been used to evaluate the possibility of using an antimony-containing intermetallic as an auxiliary electrode for an electrochemical antimony sensor.

* Electrochemical Society Active Member.
** Electrochemical Society Student Member.

Experimental

The $ZrSb_2$ for the auxiliary reference electrode was synthesized by placing antimony powder (Johnson-Matthey, 100 mesh, 99.5%) and zirconium sponge (Johnson-Matthey, 99.5%) in a molar ratio of 2.2:1 (Sb:Zr) in a quartz tube. The tube was evacuated to less than 10^3 Pa and sealed by melting the quartz with a torch. The sealed tube was held at 850°C for 24 h and then at 500°C for another 24 h. The resulting mixture of $ZrSb_2$ + Sb was then heated to 750°C in a vacuum (<10^3 Pa) for 12 h, during which time the excess Sb melted and vaporized, thus producing pure $ZrSb_2$. Samples of the resulting material were characterized with x-ray powder diffraction (XRD) using Cu K_α radiation.

Two types of stabilized zirconia tubes were used. The smaller tubes (od = 5 mm, id = 3.4 mm, length = 27.5 mm) were provided by Heraeus Electro-Nite. The larger tubes (od = 12.5 mm, id = 9 mm, length = 60 mm) were fabricated from yttria-stabilized zirconia (YSZ) powder (SEPR Ceramic Beads and Powders, 0.6 μm, 95% ZrO_2-4.6% Y_2O_3). The zirconia powder was pressed into tubes using a cold isostatic press (CIP) and then sintered at 1200°C for 24 h in air.

The experimental apparatus for the EMF measurement is shown schematically in Fig. 1. Two zirconia tubes were used for each experiment. One zirconia tube was filled with a mixture of antimony shot (Johnson-Matthey, 2 mm, 99.999%) and $ZrSb_2$. Another zirconia tube was filled with a mixture of antimony, zinc shot (Johnson-Matthey, 2 mm, 99.99%) and $ZrSb_2$. A large (12.5 mm od) zirconia tube was always used for the alloy, while either a large or small (5 mm od) tube was used for the pure antimony reference electrode. After insertion of a molybdenum wire (Johnson-Matthey, 1 mm diam) each tube was sealed with an alumina-based cement and dried. The two tubes were placed in a graphite crucible with zinc metal. The apparatus was then placed in a quartz tube through which argon gas (10^5 Pa) was passed.

The quartz tube containing the cell was heated in a vertical tube furnace. The EMF between the two tubes was measured using an HP 34401A multimeter (input impedance, 10^{10} Ω).

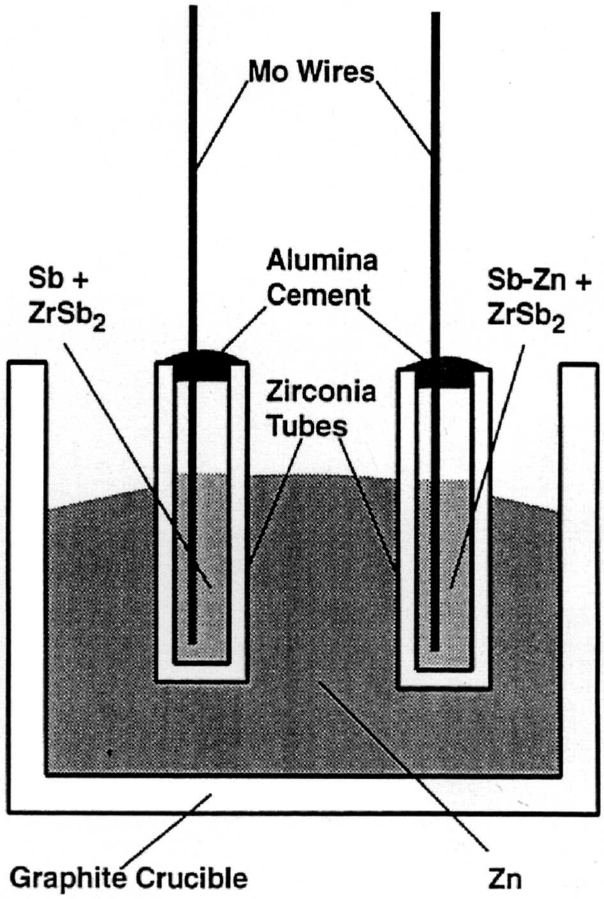

Fig. 1. Schematic diagram of experimental apparatus.

Results and Discussion

Synthesis of $ZrSb_2$.—The crystal structure of $ZrSb_2$ has been determined by Kjekshus[20] using Guinier photographs single-crystal samples. The maximum symmetry is that of the Pnnm space group and the lattice parameters are a = 14.9684 Å, b = 9.9672 Å, and c = 3.8813 Å. The Lorenz-polarization factor, the multiplicity factor, and the atomic scattering factor (data from Ref. 26) have been calculated using the 24 atomic positions given in Ref. 20. The planes for which the calculated diffraction peak intensities are 10 or greater are shown in Table I. The measured relative intensities and Bragg angles of a typical $ZrSb_2$ sample prepared as described above are also shown in Table I. Three peaks with calculated relative intensities less than 10 (indicated by [a]) were required to match all the measured peaks. The agreement between the measured and calculated values confirms the formation of $ZrSb_2$.

EMF Measurements.—The voltage between the two tubes can be described by cell I

$$\text{Sb-Zn(l)}, ZrSb_2\text{(s)} \mid \text{YSZ} \mid \text{Zn(l)} \mid \text{YSZ} \mid \text{Sb(s)}, ZrSb_2\text{(s)} \quad \text{I}$$

for which the cell voltage is given by Eq. 4 if the two tubes are at the same temperature. Since the reference electrode is pure antimony, Eq. 4 simplifies to

$$E = -\frac{RT}{2F} \ln (a_{Sb}^{alloy}) \quad [5]$$

The sensor generally produced a constant voltage within 30 min to 2 h after the furnace reached 500°C. However, after approximately 1 h or longer at a constant value, or on increasing the furnace temperature, the cell voltage decreased. The explanation for this decrease in voltage is discussed following analysis of the value of the EMF measured during initial melting of the alloy.

Initial EMF.—The constant EMF obtained after melting of the alloy shows the expected logarithmic dependence with antimony concentration as shown in Fig. 2. Although no other measurements of the antimony activity are available for comparison, the activities of antimony in molten zinc-antimony alloys have been calculated from zinc activities using the Gibbs-Duhem equation.[14] Figure 2 shows that the theoretical EMF values for cell I using the calculated antimony activities are in good agreement with the measured EMF.

The agreement between the measured EMF and the zinc activity measurement can be further demonstrated by analyzing the antimony activity coefficient (γ_{Sb}), which is defined by the antimony activity (a_{Sb}) and the antimony concentration (X_{Sb})

$$a_{Sb} = \gamma_{Sb} X_{Sb} \quad [6]$$

and thus can be calculated from the measured EMF using Eq. 5. Figure 3 shows that the activity coefficient calculated from the measured EMF from cell I is in agreement with that from the zinc activity measurements for antimony concentrations of 0.25 and less. The measured and calculated EMF values for antimony concentrations less than 0.25 can be described by the least squares regression linear curve fit, as shown in Fig. 3, which demonstrates the consistency of the two sets of results. Using this fit in Eq. 5 results in the following expression for the cell EMF at 773 K for $0.01 < X_{Sb} < 0.25$

Table I. XRD peaks for $ZrSb_2$ ($I/I_o \geq 10$).

	Calculated			Measured	
hkl	d(Å)	2θ	I/I_o	2θ	I/I_o
1 3 0	3.243	27.50	32	27.41	38
3 0 1	3.064	29.15	25	29.07	12
1 2 1	3.000	29.78	34	29.63	56
3 1 1	2.928	30.53	19	30.51	21
2 2 1	2.834	31.57	38	31.39	30
3 3 0	2.765	32.38	65	32.28	72
3 2 1	2.610	34.37	15	34.38	74
4 1 1	2.601	34.49	71	34.38	74
5 2 0	2.566	34.97	22	34.93	56
1 3 1	2.489	36.09	13	36.04	58
4 3 0	2.484	36.16	32	36.04	58
1 4 0	2.458	36.56	10	—	—
6 1 0	2.42	37.15	41	37.14	54
2 3 1	2.392	37.61	78	37.47	82
5 0 1	2.370	37.96	100	37.92	100
2 4 0	2.364	38.07	33	37.92	100
6 2 0	2.231	40.44	61	40.46	77
5 3 0	2.224	40.57	15	40.46	77
1 5 0	1.976	45.93	17	45.88	15
5 3 1	1.930	47.10	11	46.76	37
7 0 1	1.873	48.62	33	48.64	16
3 5 0	1.851	49.23	16	49.30	11
0 5 1	1.773	51.54	22	51.85	45
6 4 0	1.763	51.87	14	51.85	45
1 5 1	1.761	51.93	16	51.85	45
4 5 0	1.759	51.98	19	51.85	45
8 2 0	1.752	52.23	16	51.85	45
0 6 0	1.661	55.31	25	55.39	20
5 5 0	1.659	55.38	11	55.39	20
9 1 0	1.640	56.07	34	56.05	21
4 5 1	1.602	57.52	10	57.50	17
4 3 2	1.529	60.55	14	60.59	14
6 1 2	1.514	61.23	9[a]	61.14	17
2 4 2	1.500	61.86	15	61.80	20
7 4 1	1.497	61.99	19	62.02	24
6 2 2	1.464	63.55	31	63.57	22
2 7 0	1.399	66.90	15	66.89	18
1 5 2	1.385	67.68	10	67.78	15
4 5 2	1.303	72.53	14	72.53	18
3 7 1	1.291	73.33	14	73.53	25
10 3 1	1.287	73.58	16	73.63	20
8 5 1	1.287	73.60	11	73.63	20
10 4 0	1.283	73.87	15	73.63	20
11 1 1	1.274	74.51	10	74.52	17
0 6 2	1.262	75.32	10	75.51	20
4 7 1	1.259	75.54	11	75.51	20
9 1 2	1.253	75.96	13	75.97	14
7 6 1	1.243	76.69	10	76.73	20
8 6 0	1.242	76.73	16	76.73	20
4 1 3	1.214	78.88	6[a]	78.83	13
9 5 1	1.213	78.92	2[a]	78.83	13
5 0 3	1.188	80.96	21	81.04	12

[a] $I/I_o < 10$ required to match measured peak.

$$E_{773\,K}(\text{in mV}) = 64.6 - 45.5 \log (X_{Sb})$$

which is shown as the solid curve in Fig. 2.

Electrode stability.—As mentioned above, the cell EMF reached a constant value, but then decreased after approximately 1 h. Although the required ternary-phase diagram or thermodynamic data is not available to evaluate the stability of $ZrSb_2$ in molten zinc, hypothetical Zn-Sb-Zr phase diagrams can be constructed to illustrate the important criteria. A portion of a hypothetical isothermal section of the Zn-Sb-Zr phase diagram for a temperature greater than the melting point of pure antimony (T_m = 631°C) is shown in Fig. 4. This diagram is simpler than that for a lower temperature, but can be used to explain the reaction of $ZrSb_2$ with the molten zinc. The critical point on the diagram is the liquidus composition in the three-phase diagram which is indicated by a star in Fig. 4. The zirconium composition at this critical point represents the solubility of zirconium in the liquid. If this solubility of zirconium is large, the $ZrSb_2$ electrode dissolves into the molten alloy. The antimony composition at this point is also critical. Cell I is only sensitive to antimony for antimony concentrations higher than this critical concentration, where a two-phase equilibrium exists between the liquid and $ZrSb_2$. For concentrations lower than this critical value, $ZrZn_6$ forms and the EMF is determined by the zinc, rather than antimony, concentration.

The possible dissolution of zirconium into the Zn-Sb alloy was tested by placing either zirconium sponge or $ZrSb_2$ into a molten Zn-Sb alloy for 5 h at 700°C. The zir-

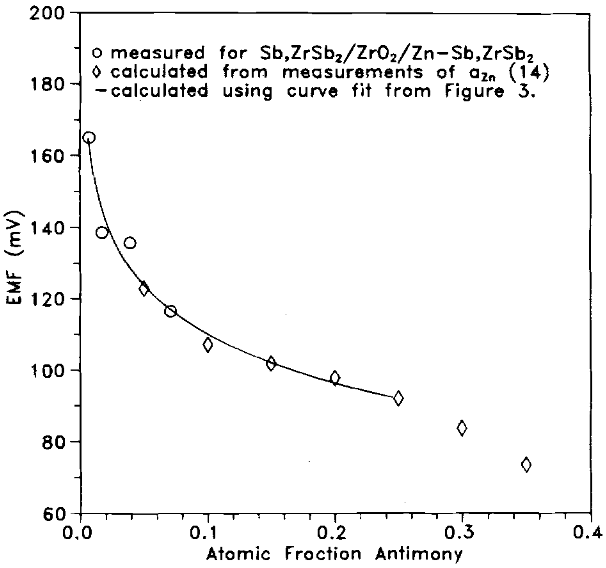

Fig. 2. Measured EMF for Cell I: Sb-Zn(l), $ZrSb_2$(s) | YSZ | Zn(l) | YSZ | Sb(s), $ZrSb_2$(s).

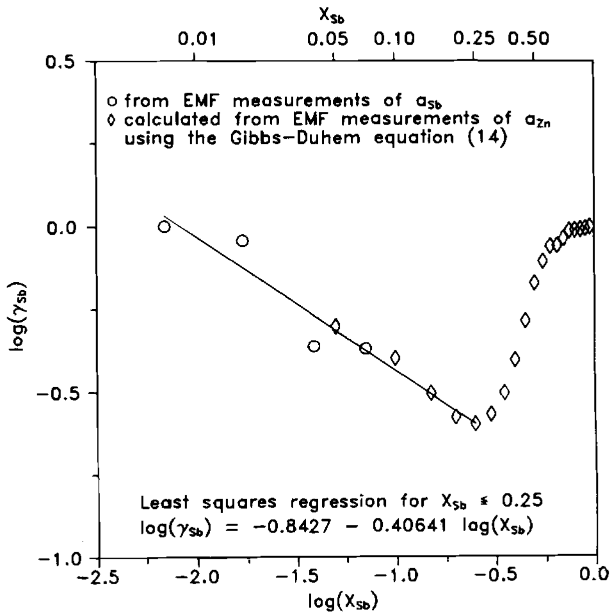

Fig. 3. Activity coefficients of antimony in molten zinc-antimony alloys.

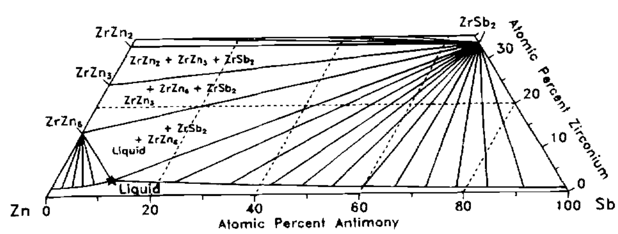

Fig. 4. A portion of an isothermal section of a hypothetical Zn-Sb-Zr phase diagram above the melting temperature of antimony.

conium sponge or $ZrSb_2$ was removed from the molten alloy, which was solidified and then analyzed using energy dispersive x-ray spectroscopy (EDS). No zirconium was detected in either solidified alloy indicating that the solubility of zirconium in molten zinc-antimony alloys is below the detection limit of EDS (1% or less).

XRD of the $ZrSb_2$ + Zn-Sb alloy mixture after the EMF experiments revealed that additional phases formed during the experiment. One additional phase was ZnO which could have formed from the residual oxygen in the argon cover gas. The presence of ZnO at the electrode/electrolyte interface could affect the oxygen pressure, and thus the sensor output. However, the ZnO was located primarily at the surface of the alloy and thus should not have affected the electrode equilibrium. More important, XRD indicated that other phases which are more likely to affect the electrode equilibrium were present. The following intermetallic compounds have been observed in the zinc-zirconium binary system: ZrZn, $ZrZn_2$, $ZrZn_3$, $ZrZn_6$, $ZrZn_{14}$, and $ZrZn_{22}$. Although JCPDS powder diffraction files are available for ZrZn and $ZrZn_2$, crystallographic data for the other compounds are available.[27,28] The additional observed peaks can be indexed to $ZrZn_3$ and $ZrZn_6$ as shown in Table II.

The formation of $ZrZn_3$ is not expected for the phase diagram shown in Fig. 4, since the average composition follows a line between the binary alloy composition and the composition of $ZrSb_2$. Such a line does not enter a phase region which contains $ZrZn_3$. However, if a three-phase equilibrium between $ZrZn_3$, $ZrZn_6$, and liquid exists, as shown in Fig. 5, a line between a zinc-rich zinc-antimony alloy and $ZrSb_2$ passes through phase regions which contain $ZrZn_3$. The critical point for operation of the sensor, as indicated by the star, is the liquid composition in the three-phase region containing $ZrSb_2$. At temperatures below 545°C, an additional compound exists in the zirconium-zinc system ($ZrZn_{14}$).[27] The existence of $ZrZn_{14}$ results in an additional three-phase triangle in the zinc-rich corner of the ternary diagram. However, the presence of $ZrZn_3$ and $ZrZn_6$ according to the XRD results indicate that $ZrZn_{14}$ is not in equilibrium with $ZrSb_2$, so the critical point is still the liquid composition in equilibrium with $ZrSb_2$ and $ZrZn_3$.

The formation of $ZrZn_x$ ($ZrZn_3$, $ZrZn_6$, or $ZrZn_{14}$) by the following reaction

$$ZrSb_2 + xZn = ZrZn_x + 2Sb \qquad [8]$$

Table II. Additional XRD peaks from the reaction of $ZrSb_2$ with molten zinc.

Observed peak	$ZrZn_3$ cubic a = 16.3 Å		$ZrZn_6$ body-centered tetragonal a = 12.70 Å, b = 8.68 Å	
2θ	hkl	2θ	hkl	2θ
30.40			3 1 2	30.33
38.25	4 4 4	38.26		
45.88	6 4 4 0 2 8	45.92		
53.40	4 5 7 1 5 8 0 3 9	53.32		
56.27			4 5 3	56.24
57.93	4 5 8 1 2 10	57.98		
61.36			4 1 5	61.30
68.89			3 1 6	69.01
73.63	4 8 9 5 6 10 1 4 12 2 6 11	73.77		
75.51	2 8 10	75.63		
77.06	2 5 12 3 8 10 4 6 11 0 2 13	76.95		
79.94	2 6 12	79.82		

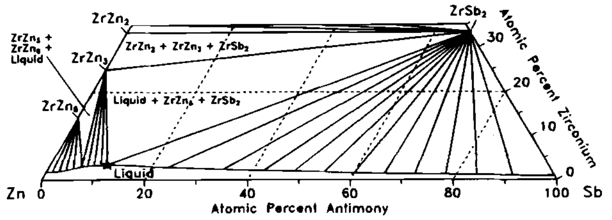

Fig. 5. A portion of an isothermal section of a hypothetical Zn-Sb-Zr phase diagram above the melting temperature of antimony which is consistent with the formation of $ZrZn_3$.

could affect the cell voltage in two ways. One effect is that the antimony produced by reaction 8 will increase the antimony concentration in the alloy and thus affect the cell voltage. The other, more important effect, is that the equilibrium between $ZrZn_x$ and molten zinc will establish the oxygen partial pressure at the working electrode, so the cell voltage will respond to zinc rather than to antimony.

Conclusion

A galvanic cell for measuring the antimony concentration in molten zinc-antimony alloys has been developed using a stabilized zirconia solid electrolyte with a $ZrSb_2$ auxiliary electrode to provide the sensitivity to antimony. The measured EMF values are in agreement with results calculated from EMF measurements of the zinc activity in zinc-antimony alloys. However, the sensitivity of the cell to antimony is lost on formation of a zirconium-zinc intermetallic compound ($ZrZn_3$ or $ZrZn_6$), which occurs in alloys with antimony concentrations below a critical value. The results in this work indicate that this critical antimony concentration is at least 7 atomic percent Sb, which is much larger than the antimony concentrations in zinc alloys during hot-dip galvanization (0.01 to 0.1%). Thus, the sensor would have a short lifetime in a hot-dip galvanization zinc bath and thus could only be used, at best, for a disposable antimony sensor in hot-dip galvanization. The sensor could possibly have a longer lifetime in zinc alloys with higher antimony concentrations or in other antimony-containing alloys which do not react with $ZrSb_2$ to form intermetallic compounds.

Acknowledgments

The authors are grateful to Richard Conti of Heraeus Electro-Nite who provided the small zirconia tubes and to SEPR Ceramic Beads and Powders for providing the yttria-stabilized zirconia powder.

Manuscript submitted Dec. 11, 1995; revised manuscript received April 6, 1996.

Auburn University assisted in meeting the publication costs of this article.

REFERENCES

1. S. Chang and J. C. Shin, *Corros. Sci.*, **36**, 1425 (1994).
2. J. N. Pratt, *Metall. Trans. A*, **21A**, 1223 (1990).
3. S. Srikanth and K. T. Jacob, *Mater. Sci. Technol.*, **5**, 427 (1989).
4. S. K. Hahn and D. A. Stevenson, *J. Chem. Thermodyn.*, **11**, 627 (1979).
5. S. Anik and M. G. Frohberg, *Ber. Bunsen-Ges. Phys. Chem.*, **91**, 790 (1987).
6. S.-A. Cho, R. Camisotti, and M. H. Velez, *Metall. Trans. B*, **21B**, 87 (1990).
7. V. G. Ryabov and I. T. Sryvalin, *Russ. Metall.*, **2**, 51 (1971).
8. X. Y. Yan, D. E. Lanberg, and W. J. Rankin, *Metall. Trans. B*, **24B**, 1037 (1993).
9. T. D. Van, L. Segers and R. Winand, *This Journal*, **141**, 927 (1994).
10. E. T. Turkdogan, *Physical Chemistry of High Temperature Technology*, Academic Press, New York (1980).
11. T. Senda and R. C. Bradt, *J. Am. Ceram. Soc.*, **74**, 1296 (1991).

12. J. Bruley, U. Bremer, and V. Kraševec, *ibid.*, **75**, 3127 (1992).
13. V. Kraševec, M. Tronteki, and L. Golič, *ibid.*, **74**, 760 (1991).
14. I. B. Rubin, K. L. Komarek, and E. Miller, *Z. Metallkde.*, **65**, 191 (1974).
15. A. Mikula, *Metall. Trans. B*, **23B**, 601 (1992).
16. V. I. Posypaiko and E. A. Alekseeva, *Phase Equilibria in Binary Halides*, IFI/Plenum, New York (1987).
17. E. Garcia and J. D. Corbett, *Inorg. Chem.*, **29**, 3274 (1990).
18. E. Garcia and J. D. Corbett, *J. Solid State Chem.*, **73**, 440 (1988).
19. E. Garcia and J. D. Corbett, *ibid.*, **73**, 452 (1988).
20. A. Kjekshus, *Acta Chem. Scand.*, **26**, 1633 (1972).
21. A. K. Ganguli, Y.-U. Kwon, and J. L. Corbett, *Inorg. Chem.*, **32**, 4354 (1993).
22. D. J. Min and N. Sano, *Metall. Trans. B*, **20B**, 863 (1989).
23. K. Deller and B. Eisenmann, *Z. Naturforsch.*, **31b**, 29 (1976).
24. K. Deller and B. Eisenmann, *ibid.*, **33b**, 676 (1978).
25. E. Brechtel, G. Cordier, and H. Shäfer, *ibid.*, **36b**, 1341 (1981).
26. C. H. MacGillavry and G. D. Rieck, *International Tables for X-Ray Crystallography. Volume III: Physical and Chemical Tables*, The Kynoch Press, Birmingham, England (1962).
27. P. Chiotti and G. R. Kilp, *Trans. Metall. Soc. AIME*, **215**, 892 (1959).
28. S. Samson, *Acta Crystallogr.*, **14**, 1229 (1961).

Surface Electronic Structures and Photoluminescence Mechanisms of Porous Si

Yoshiyuki Suda,[a] Tomohiro Koizumi,[a] Koji Obata,[a] Yasuhisa Tezuka,[b] Shik Shin,[b] and Nobuyoshi Koshida[a]

[a]*Faculty of Technology, Tokyo University of Agriculture and Technology, 2-24-16 Naka-cho, Koganei, Tokyo 184, Japan*
[b]*Institute for Solid State Physics, The University of Tokyo, 3-2-1 Midori-cho, Tanashi, Tokyo 188, Japan*

ABSTRACT

Surface structures and photoluminescence (PL) mechanisms of porous Si (PS) and the role of oxygen termination on PS have been investigated using a synchrotron-radiation photoemission spectroscopy technique, an Auger electron spectroscopy technique, and a photoluminescence technique. There is almost no trace of oxygen on the surface of as-anodized PS and its surface is covered with hydrides. An increase in PL intensity with increasing anodization current is interpreted to correspond to an increase in the number of photoluminescent elements. The investigation on the oxidation effect suggests that oxygen termination itself does not affect electronic transition levels unless it modifies the size or the structure of the Si crystallites. Energy bandgap analysis indicates that PL peak energy of PS correlates well to the surface energy gap, and that values of energy gaps and exciton energies obtained for PS are close to the results of the recent theoretical calculations for quantum dots and wires.

Introduction

The origin of visible photoluminescence (PL) in porous Si (PS) is still controversial, though many researchers have ascribed it to Si microstructures including bandgap quantization originating from Si crystallites. Quantum-size structures including dot shapes and wire shapes with a diameter of 2 ~ 4 nm have been experimentally reported using a transmission electron microscopy (TEM) technique,[1,2] a scanning tunneling microscopy (STM) technique,[3,4] and a Raman spectroscopy technique.[5,6] The results of theoretical calculations[7,8] also indicate that quantum dots and quantum wires of almost the same size have the minimum transition energies which correspond to the peak energies of PL from porous Si in consideration of exciton energies. The results of a vacuum-ultraviolet reflection measurement[9] and an electron spin resonance (ESR) measurement[10] indicate that PS possesses a crystalline property rather than an amorphous property. In early works on PS, surface hydrides,[11,12] oxides,[13] and their composites[14] have been reported to be deeply related to the luminescence process. Thus, the surface characterization of PS is essential to distinguish the surface effects from the bulk effects on the PL mechanisms and to understand the PL origin.

In recent years, most studies on surface hydrides on PS,[15-18] including our report,[19] have indicated almost no relation between the surface hydrides and the PL properties. In this paper, on the basis of this result, we have investigated if oxygen exists on the surface of PS crystallites and the role of oxygen bonding in the PL mechanism. First, the surface structure of an as-anodized freshly prepared PS surface has been characterized. Then, to investigate the effect of oxygen bonding in PS on the PL mechanism, two oxidation methods have been carried out. In the first method, as-anodized PS was kept in the same anodization solution under 500 W tungsten light exposure, which is hereafter called a light exposure treatment.[20] In the second method, as-anodized PS was exposed to oxygen excited by electron impact, which is hereafter called a dry oxidation treatment.

Oxygen easily bonds to a Si surface in the air. Thus, to prevent a PS surface from being unexpectedly contaminated with oxygen, we have used vacuum systems for both PL measurements and surface characterizations, and PS surfaces were kept unexposed to air from the beginning of their preparation to the end of the measurement. This method has been described in our previous paper.[21] For the surface characterization, we have used a synchrotron-radiation photoemission spectroscopy (SRPES) and Auger electron spectroscopy (AES) techniques, and have analyzed the surface compositions, the valence and core electronic states, and the energy bandgaps of as-anodized PS and the oxidation-treated PS. These results of the surface structures and the electronic states have been compared to the corresponding PL properties and the PL origin and the role of the oxygen bonding have been discussed.

Experimental

PS samples were prepared by anodizing p-type 2 ~ 6 Ω-cm (001) Si wafers in a mixture of 55 weight percent (w/o) aqueous HF solution and ethanol at anodization current densities of 10 to 200 mA/cm^2 (as-anodized PS). These sample preparations were completed in a dark room. To investigate the effect of oxygen bonding in PS on the PL mechanism, as-anodized PS samples have been treated with two oxidation methods: a light exposure treatment and a dry oxidation treatment. In the light exposure treatment, as-anodized PS samples, formed at an anodization